Genes & Diseases (2024) 11, 101231

Available online at www.sciencedirect.com

ScienceDirect

journal homepage: www.keaipublishing.com/en/journals/genes-diseases

RAPID COMMUNICATION

MMP-9 deficiency accelerates the progress of periodontitis

Periodontitis is a chronic inflammatory disease caused by periodontopathic bacteria that affects periodontal support tissues.[1] If left untreated, it results in loss of periodontal attachment and alveolar bone resorption. Approximately one-half of adults in the United States older than 30 years have periodontal disease.[2] Though the disease is initiated by bacterial infection, it activates host defense systems that eventually lead to the degradation of the periodontium. During periodontitis, the disease progress involves further production of pro-inflammatory mediators such as cytokines, proteolytic enzymes like matrix metalloproteinases (MMPs), and their inhibitors.

MMP-9 is one of the MMPs[1] capable of processing collagen and non-collagen proteins and plays diverse roles in physiological and pathological development. It promotes inflammation in tissues and diseases such as periodontitis. High MMP-9 expression was observed in periodontal diseases. However, several reports demonstrated that MMP-9 is not related to periodontitis.[3] In contrast, *MMP-9* mutations in humans are associated with metaphyseal anadysplasia (OMIM 613073) and skeletal defects.[4] MMP-9 overexpression attenuates osteoclast (OC) formation and inhibits pro-inflammatory cytokines secretion. *MMP-9* knockout (KO) mice develop severe periapical lesions with inflammation.[5] This indicates that MMP-9 has dual effects on physiological and pathological development. How MMP-9 regulates alveolar bone metabolism and periodontium during aging has not been described. This study aimed to investigate the effect of MMP-9 on the balance of osteogenesis and osteoclastogenesis in periodontium with aging.

We found that *MMP-9* KO mice gradually develop deteriorated periodontic tissues with aging. X-ray radiography and micro-computed tomography (μCT) revealed a striking alveolar bone loss in molar mandibular furcation and interdental region of *MMP-9* KO mice at 6, 12, and 29 months old compared with controls (Fig. 1A–C). Noticeably, the destruction of alveolar bone in *MMP-9* KO mice was more evident with aging. Obvious space in the apical region on the alveolar bone was observed in 12- and 29-month-old *MMP-9* KO mice. Hyper-mineralized deposits were observed in the alveolar bone of 29-month-old *MMP-9* KO mice. Bone mineral density of alveolar bone of 2-, 6-, 12-, and 29-month-old *MMP-9* KO mice was also reduced (Fig. 1C). With aging, loss of alveolar bone was gradually prominent in *MMP-9* KO. Additionally, molar cusps in *MMP-9* KO groups at 6, 12, and 29 months old were worn (Fig. S2). Scanning electron microscopy (SEM) using backscattered electrons also displayed more alveolar bone loss and bone resorption in interdental, furcation, and periapical regions in *MMP-9* null mice, especially apical regions of alveolar bone with aging (Fig. S3).

To further evaluate the morphological changes in osteocytes and the lacunae-canalicular structures within the alveolar bone, we employed acid-etched SEM. Our examination encompassed 2-, 6-, 12-, and 29-month-old *MMP-9* KO mice. SEM images captured at low and middle magnifications (500 μm and 200 μm) revealed evident trabecular bone resorption, with pronounced large lacunae-canalicular structures prominently present in the apical regions of the alveolar bones, particularly in the 6-, 12-, and 29-month-old *MMP-9* KO mice. Upon closer inspection at high magnification (50 μm), we observed a diminished number of unevenly distributed and irregularly spaced osteocytes in the mutant mice, especially among the aged *MMP-9* KO mice. In contrast, osteocytes in the alveolar bones of wild-type mice exhibited a highly organized and evenly dispersed pattern, with distinct outlines. Furthermore, in the 29-month-old *MMP-9* KO mice, SEM imaging revealed the deposition of calcium within the trabecular bones (Fig. 1D). These findings suggest that MMP-9 may play a multifaceted role encompassing the regulation of mineralization and the formation and/or maintenance of osteogenesis. The region of interest was evaluated by two- and three-dimensional reconstructions using μCT analysis. Quantitative data analyses revealed bone volume, bone volume/tissue volume, and trabecular thickness in the first molar alveolar bone were significantly low at 6-, 12- and 29-

Peer review under responsibility of Chongqing Medical University.

https://doi.org/10.1016/j.gendis.2024.101231

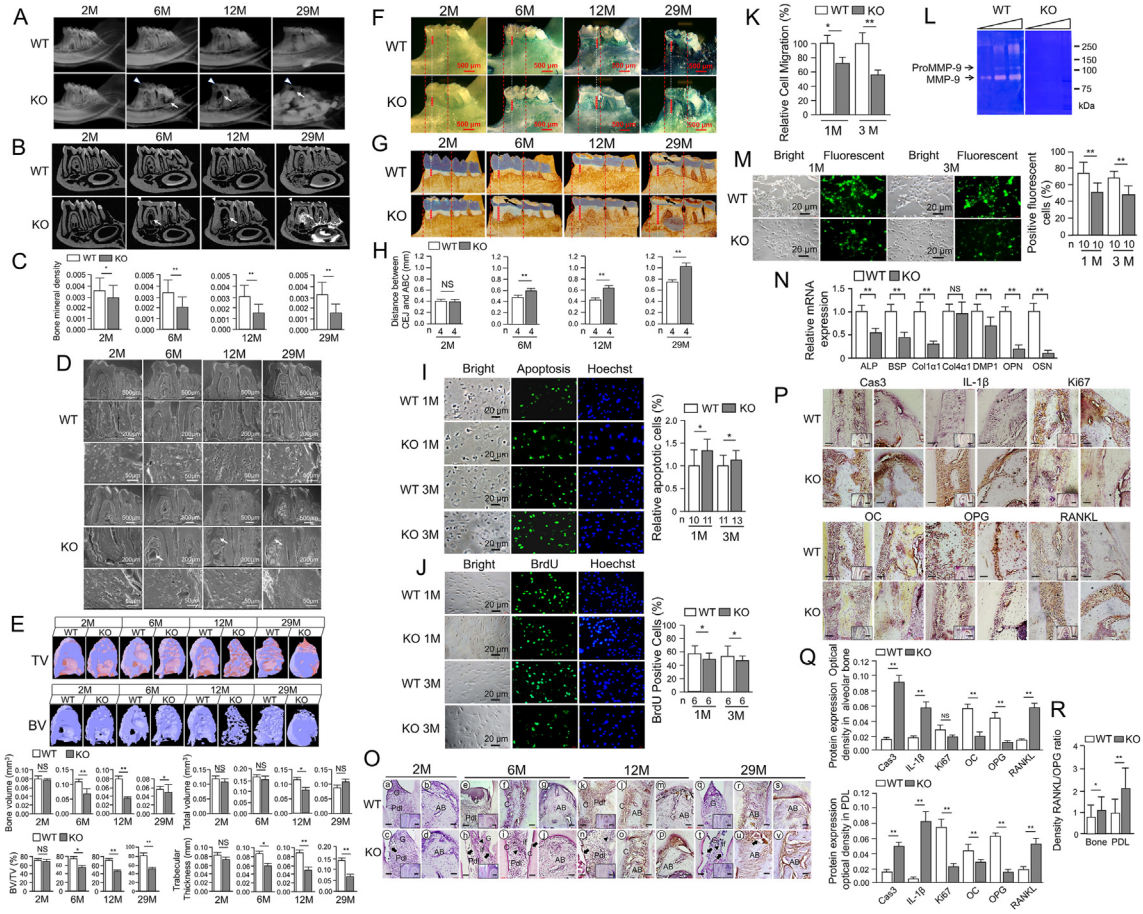

Figure 1 MMP-9 deficiency impairs bone metabolism and cell proliferation as well as causes inflammation in the periodontium. **(A)** Representative radiographs show an overall reduction of the mineralization of the alveolar bone and loss of the alveolar bone in the root furcation regions (arrows) of the MMP-9 KO mice at 6, 12, and 29 months old, and the alveolar bone was porous in the apical space in the furcation regions. Molar cusps (arrowheads) were severely attrited in MMP-9 KO mice at these ages. **(B)** μCT shows that BMD of the alveolar bone of MMP-9 KO mice was decreased compared with the control groups. With aging, the alveolar bone resorption in the alveolar bone of MMP-9 KO mice was more severe. A porous region (arrows) in the apical areas was seen. Hyper-mineralized spots were deposited on the alveolar bones in 29-month-old MMP-9 KO mice. **(C)** Graph representation of BMD in the wild-type and MMP-9 KO mice acts as mean ± standard error of the mean. **(D)** Resin infiltration and acid etching SEM analysis revealed noteworthy findings in the alveolar bone of 2-, 6-, 12-, and 29-month-old MMP-9 knockout (KO) mice. Within the apical regions of the alveolar bone, trabecular bones displayed clear evidence of bone resorption, leading to porous spaces in the mutant mice. Additionally, calcium deposition was observed in the trabecular bones of 29-month-old MMP-9 KO mice. In 2-month-old wild-type mice, osteocytes within the trabecular bones exhibited an even distribution, whereas osteocytes in the alveolar bone of the same age MMP-9 KO mice displayed less organization. As aging progressed, the number of osteocytes in the trabecular bones of MMP-9 KO mice decreased, accompanied by an increase in matrix presence. Conversely, osteocytes and lacunae structures in the alveolar bones of age-matched control groups remained highly organized and uniformly distributed. **(E)** μCT analyzed alveolar bone microstructure parameters in the wild-type and *MMP-9* KO mice. TV and BV on the alveolar bone were from the wild-type and *MMP-9* KO mice at 2-, 6-, 12-, and 29-month-old. Quantitative trabecular bone significantly reduced BV, BV/TV, and Tb. Th. in *MMP-9* KO mice at 6-, 12- and 29-month-old. BV, bone volume; TV, tissue volume; BV/TV, bone volume/tissue volume; Tb. Th., trabecular thickness. NS, no significance. **(F)** Alveolar bone loss by the linear CEJ-ABC distance was measured by a stereomicroscope. The samples were stained with methylene blue to reveal the CEJ. Teeth were worn in the *MMP-9* KO mice (arrows). CEJ, cemental-enamel junction; ABC, alveolar bone crest. **(G)** Distance from the CEJ to the ABC in the wild-type and *MMP-9* KO mice was measured by μCT. **(H)** Graphical representations of CEJ to ABC were measured as mean ± standard error of the mean ($n = 4$). **(I)** Apoptotic cells in the primary BMSCs. A fluorescent terminal deoxynucleotidyl transferase (TdT) assay was used for detection of apoptotic cells (green) in cultured BMSCs from 1- and 3-month-old wild-type and *MMP-9* KO mice was performed. Hoechst was used for nucleus staining (Blue). Bar = 20 μm. Relative apoptotic cells in the BMSCs from the wild-type and null mice were shown. The expression of apoptotic cells from the wild-type mice acted as a 1.0. **(J)** Cell proliferation of the BMSCs from the 1- and 3-month-old wild-type and *MMP-9* KO mice was observed. Cell proliferation was identified by BrdU incorporation. Cells were transferred into four-well glass slides and incubated with 30 mM BrdU in a culture medium for 6 h. The cells were treated with an anti-BrdU antibody, followed by the secondary antibody with Alexa Fluo® 488 green. For nucleus staining, the cells were incubated with a

month-old in *MMP-9* KO mice (Fig. 1E). In addition to bone mineral density, bone volume, bone volume/tissue volume, and trabecular thickness, bone surface density, bone surface/volume ratio, closed porosity, number of closed pores, open porosity percent, surface closed pores, total apparent mineral density, total pores, total surface, trabecular number, volume of closed pores, and volume of open pore space were measured and calculated by μCT analysis (Fig. S4). Bone surface density, total apparent mineral density, trabecular number, and volume of open pore space in 29-month-old *MMP-9* KO mice were remarkably reduced (Fig. S4A–D). The quantitative μCT data displayed a significant increase in open porosity percent and total pores in 6-, 12-, and 29-month-old *MMP-9* KO mice (Fig. S4E, F). Furthermore, the bone surface/volume ratio on the alveolar bone of the 6-, and 12-month-old *MMP-9* KO mice was higher than the wild-type mice (Fig. S4G). Total surface on the alveolar bone in 12-, and 29-month-old *MMP-9* KO mice was lower than that of age-matched wild-type mice (Fig. S4H). Closed porosity, number of closed pores, surface closed pores, and volume of closed pores on the alveolar bone exhibited a reduction in all ages of *MMP-9* KO mice (Fig. S4I–L). This result demonstrated that *MMP-9* KO causes osseous destruction of alveolar bones.

Stereomicroscopic and μCT analyses revealed that *MMP-9* KO groups at 6, 12, and 29 months old exhibited a more dramatic increase in distance from the cemental-enamel junction to the alveolar bone crest compared with wild-type mice (Fig. 1F–H). Noticeably, the distance from the cemental-enamel junction to the alveolar bone crest gradually increased with aging in *MMP-9* KO groups.

To assess the effect of MMP-9 on cell apoptosis, proliferation, migration, and extracellular matrix remodeling, primary bone marrow stromal cells (BMSCs) isolated from 1- and 3-month-old wild-type and *MMP-9* KO mice were chosen for this study. Compared with the wild-type groups, the rate of cell apoptosis was higher in *MMP-9* KO groups (Fig. 1I), whereas cell proliferation was reduced in *MMP-9* KO groups (Fig. 1J). Next, cell migration was measured by BioCoatTM Matrigel Invasion Chamber assay. This result showed that BMSCs from *MMP-9* KO mice displayed reduced cell migration compared with the wild-type cells (Fig. 1K).

As MMP-9 is capable of remodeling extracellular matrix, we examined whether MMP-9 processes gelatin and collagen type 4 (Col4). This result showed that the bands catalyzed by MMP-9 from the wild-type tissues were intense with high molecular weight bands ranging from approximately 200 to 86 kDa of pro-MMP-9 and MMP-9 proteins

1:5000 dilution of Hoechst. Images were obtained with a Nikon inverted microscope. Proliferative cells were expressed as a percentage of the number of BrdU-positive cells relative to the total number of Hoechst-positive nuclei. **(K)** Analysis of cell migration from wild-type and *MMP-9* null mice. Migration of the BMSCs from wild-type and *MMP-9* KO mice was measured using BD BiocoatTM Matrigel invasion chambers. Cell migration was quantified by counting the number of cell migrants passing through the membranes after 12 h. The wild-type cell migration was set as 100 %. **(L)** Functional role of the wild-type and *MMP-9* mutant cells by gelatin zymography. Increases in MMP-9 levels from the wild-type cells catalyze gelatin with increasing MMP-9 concentrations whereas in *MMP-9* KO cells failed to process gelatin. **(M)** *In situ* zymography of MMP-9 activity on its substrate in vivo. The BMSCs isolated from the wild-type and *MMP-9* KO mice were grown on DQ-fluorescent Col4-coated slides for 12 h. The cells were fixed and images were observed under an immunofluorescent inverted microscope. Data showed that the number and intensity of Col4 degradation in the wild-type cells were higher than those of the *MMP-9* null cells. The percentage of positive fluorescent spots in the BMSCs from the wild-type and MMP-9 KO mice was obtained. "*n*" indicates the number of animals used in each group. **(N)** Quantitative reverse transcription PCR analysis revealed that mRNA expression levels of *ALP*, *BSP*, *Col1α1*, *DMP1*, *OPN*, and *OSN* in BMSCs from 3-month-old *MMP-9* null mice were significantly reduced when compared with age-matched wild-type mice. However, there was no significant difference in the expression of *Col4α1* in BMSCs between the wild-type and *MMP-9* KO mice. The data were presented as the mean ± standard deviation ($n = 4$). *$P < 0.05$ and **$P < 0.01$. Details of the primers used in this study are shown in Table S1. **(O)** Hematoxylin and eosin staining of periodontal tissues in the wild-type and *MMP-9* KO mice. *MMP-9* KO mice had progressive periodontal diseases with aging. (c, d) Higher magnification views from the boxed area in 2-month-old *MMP-9* KO mice. Gingival epithelium and PDL had torn away from the cementum. There was no remarkable difference in the alveolar bone of the wild-type versus *MMP-9* KO mice. (a, b) Higher magnification views from the boxed area in 2-month-old wild-type mice. (h–j, n–p) Higher magnification from the boxed areas in 6-, and 12-month-old *MMP-9* null mice. The gingival membrane and PDL were severely detached from the cementum (arrows). Inflammation was seen in the periodontal tissue and alveolar bone resorption was present in *MMP-9* KO mice (arrowheads). (e–g, k–m) Higher magnification views of the alveolar bone were from the boxed areas in 6- and 12-month-old wild-type mice. (t–v) Higher magnification views of the boxed area in 29-month-old *MMP-9* KO mice showed periodontal tissue destruction and detachment of gingival epithelium and PDL from the cementum. Inflammation was noted in the periodontal tissue. Cement structure was abnormal, and bone resorption was observed in the alveolar bones in *MMP-9 KO* mice. (q–s) Higher magnification views from the boxed area in 29-month-old wild-type samples. AB, alveolar bone; C, cementum; G, gingival membrane; If, inflammatory cells; PDL, periodontal ligament. Bars, 50 μm. Bars in boxes, 200 μm. **(P)** Immunohistochemistry analysis of caspase 3, IL-1β, Ki67, osteoclast (OC), osteoprotegerin (OPG), and RANKL in the periodontal tissues of the wild-type and MMP-9 KO mice. A higher magnification image of the boxed areas shows the expression of caspase-3, IL-1β, Ki67, OC, OPG, and RANKL proteins in the wild-type and MMP-9 KO teeth. **(Q)** Graph representation demonstrated protein density as mean ± standard error of the mean in the alveolar bone of the wild-type and *MMP-9* KO mice. The quantitative analysis of caspase-3, IL-1β, Ki67, OC, OPG, and RANKL protein detection in the periodontal tissues of the wild-type and *MMP-9* KO mice was shown. **(R)** The RANKL/OPG ratio in the alveolar bone and PDL of the wild-type and *MMP-9* KO mice was determined. BMD, bone mineral density; BMSCs, bone marrow stromal cells; Cas3, caspase-3; μCT, micro-computed tomography; M, month; n, number; KO, knockout; WT, wild type; *$P < 0.05$; **$P < 0.01$.

analyzed by gelatin zymography, while *MMP-9* deletion failed to degrade gelatin (Fig. 1L). *In vivo* study showed that the BMSCs from the wild-type mice highly processed Col4 compared with that of *MMP-9* mutant mice (Fig. 1M). Expression levels of osteogenic genes were reduced in BMSCs from 3-month-old *MMP-9* null mice including *ALP*, *BSP*, *Col1α1*, *DMP1*, *OPN*, and *OSN* compared with the age-matched wild-type mice (Fig. 1N).

Tissue morphology revealed that gingival tissue and periodontal ligament (PDL) in *MMP-9* null mice had torn away from the cementum, and tissue degradation around the torn area was present in *MMP-9* KO mice (Fig. 1O). With aging, extensive levels of alveolar bone loss, inflammation, and periodontal defects were much worse. Additionally, porous spaces near the cementum and several cracks around the alveolar bone were seen (Fig. 1P).

The immunostaining assay showed a stronger IL-1β signal in PDL and alveolar bone of *MMP-9* KO mice than that of the wild-type mice (Fig. 1P, Q). Expression of RANKL and caspase-3 was higher in the alveolar bone and PDL regions in the mutant mice (Fig. 1P, Q). In contrast, the expression of OC and osteoprotegerin (OPG) within PDL and alveolar bone in *MMP-9* KO mice was lower than that in the wild-type mice (Fig. 1P, Q). RANKL/OPG ratio was up-regulated in *MMP-9* KO mice compared with the wild-type mice (Fig. 1R). The immunostaining analyses showed that the expression of Ki67, a cell proliferation marker, was reduced in PDL of *MMP-9* KO mice compared with the control mice (Fig. 1P, Q).

Conclusively, our study revealed that loss of *MMP-9* resulted in enhanced periodontal inflammation and bone destruction in the periodontium. Osteogenic gene expression was reduced in BMSCs from 3-month-old *MMP-9* mutant mice. Increased expression of IL-1β, caspase-3, and RANKL, and decreased expression of Ki67, OC, and OPG in the alveolar bone and PDL in *MMP-9* KO mice caused an imbalance between cell proliferation, apoptosis, and bone metabolism. Also, the RANKL/OPG ratio and inflammatory response were increased in *MMP-9* null mice. The results indicated that MMP-9 plays dual effects (gain- or loss-function) on maintaining periodontium by regulating the balance between bone formation, bone resorption, and inflammation. However, the mechanisms of MMP-9 in periodontitis are not clearly understood, further study is needed to uncover the exact mechanisms of MMP-9 in osteogenesis and osteoclastogenesis.

Ethics declaration

All animal experiments were approved by the Institutional Animal Care and Use Committee (IACUC; approval number: 20050012AR) by the University of Texas Health Science Center in San Antonio, Texas, USA.

Author contributions

Study conception and design: C.-Y.W. and S.C.; Article drafting and revision: C.-Y.W., G.G., and S.C.; Experimental design and performance: C.-Y.W., X.-Y.L., Y.Y., W.-A.X., D.-S., Ste. C., and S.C.; Data analysis: C.-Y.W., G.G., M.M.L., F.W., Z.C., L.A.C., and S.C.; Supervision: M.M., Z.C., M.L., and S.C.; Article drafting and revision: C.-Y.W., G.G., and S.C. All authors read and agreed to the published version of the manuscript.

Conflict of interests

The authors declared no conflict of interests.

Funding

This work was supported by the National Institutes of Health grants, RO1DE019802, the Pilot Grant of the School of Dentistry, UTHSCSA, 131314.

Acknowledgements

We thank Dr. Roberto Fajardo and Mr. James Schmitz (RAYO, the Center for Bone and Mineral Imaging, Department of Orthopedics, UTHSCSA) for performing micro-computed tomography imaging.

Appendix A. Supplementary data

Supplementary data to this article can be found online at https://doi.org/10.1016/j.gendis.2024.101231.

References

1. Tan J, Dai A, Pan L, et al. Inflamm-aging-related cytokines of IL-17 and IFN-γ accelerate osteoclastogenesis and periodontal destruction. *J Immunol Res*. 2021;2021:9919024.
2. Michaud DS, Fu Z, Shi J, Chung M. Periodontal disease, tooth loss, and cancer risk. *Epidemiol Rev*. 2017;39(1):49–58.
3. Razavi P, Rezaee SA, Akhondian S, Asgari N, Fatemi K, Mohajertehran F. Matrix metalloproteinase-3 but not matrix metalloproteinase-9, implicated in the manifestation of chronic periodontitis. *Rep Biochem Mol Biol*. 2023;11(4):656–662.
4. Sharony R, Borochowitz Z, Cohen L, et al. Prenatal course of metaphyseal anadysplasia associated with homozygous mutation in MMP9 identified by exome sequencing. *Clin Genet*. 2017;92(6):645–648.
5. Wan C, Yuan G, Yang J, et al. MMP9 deficiency increased the size of experimentally induced apical periodontitis. *J Endod*. 2014;40(5):658–664.

Chun-Yan Wan [a,b], Yixin Yin [b,c], Xiaoyan Li [b,d], Meng Meng Liu [b], Graham Goldman [b], Li-An Wu [b,e], Feng Wang [b,f], Dao-Shu Luo [b,f], Zhuo Chen [b,g], Wen-An Xu [b,h], Stephen Chen [b], Mary MacDougall [i], Merry L. Lindsey [j], Zhi Chen [k], Shuo Chen [b,*]

[a] *Department of Endodontics, The Affiliated Hospital of Qingdao University, School of Stomatology, Qingdao University, Qingdao, Shandong 266003, China*
[b] *Department of Developmental Dentistry, School of Dentistry, The University of Texas Health Science Center at San Antonio, San Antonio, TX 78229, USA*
[c] *Oral Implantology Center, Jinan Stomatological Hospital, Jinan, Shandong 250001, China*
[d] *Department of Endodontics, School and Hospital of Stomatology, Cheeloo College of Medicine, Shandong Key Laboratory of Oral Tissue Regeneration, Shandong*

Engineering Laboratory for Dental Materials and Oral Tissue Regeneration, Shandong University, Jinan, Shandong 250012, China
[e] *Department of Pediatric Dentistry, School of Stomatology, The Fourth Military Medical University, Xi'an, Shaanxi 710032, China*
[f] *Laboratory of Clinical Applied Anatomy, Department of Human Anatomy, School of Basic Medical Sciences, Fujian Medical University, Fuzhou, Fujian 350108, China*
[g] *Key Laboratory for Oral Biomedical Research of Zhejiang Province, Affiliated Hospital of Stomatology, Medical College, Zhejiang University, Hangzhou, Zhejiang 310027, China*
[h] *Department of Stomatology, Nanfang Hospital, Southern Medical University, Guangzhou, Guangdong 510515, China*
[i] *UBC Faculty of Dentistry, University of British Columbia, Vancouver, BC V6T 1Z3, Canada*
[j] *School of Graduate Studies and Research, Meharry Medical College and Research Biologist, Research Service Nashville VA Medical Center, Nashville, TN 37208, USA*
[k] *State Key Laboratory Breeding Base of Basic Science of Stomatology (Hubei- MOST), Key Laboratory for Oral Biomedicine of Ministry of Education (KLOBM), School and Hospital of Stomatology, Wuhan University, Wuhan, Hubei 430079, China*

*Corresponding author. Tel.: +1 210 567 3511.
E-mail address: chens0@uthscsa.edu (S. Chen)
26 July 2022
Available online 28 January 2024